Observed frequency and intensity of tropical precipitation from instantaneous estimates.

Michela Biasutti and Sandra E. Yuter

ABSTRACT

Negative societal impacts can result from intense individual downpours, the accumulation of rainfall over a day or more, or a combination of these. Accumulation is reasonably well captured by daily reporting rain gauges, but rainfall intensity is not. The Tropical Rainfall Measuring Mission (TRMM) Precipitation Radar (PR) permit description of the spatial and seasonal distributions of rainfall intensity at the timescales of the individual convective events—and permit an emphasis on how these distributions differ from the distributions of mean daily accumulation.

Over tropical land, mean rainfall intensity is highest just before the rainiest time of year (when rainfall is most frequent). The contrast is most obvious in pre-onset and post-onset months in monsoon regions, but it is also evident in regions without a well defined dry and rainy season, such as equatorial regions. Most seasonal variations in rainfall intensity can be explained as parallel variations in the occurrence of convective, relative to stratiform, precipitation. However, regional differences in rainfall intensity are related to difference in the intensity of convection itself.

Compared with seasonal changes in intensity over land, variations in convective fraction over tropical oceans are trivial, and the modest seasonal changes in the intensity of rainfall parallel those of frequency.

These findings suggests that studies of precipitation extremes under global warming should (1) explicitly tackle the question of changes in the intensity of rainfall separately from changes in daily

rainfall accumulation and (2) consider the different qualities of extreme precipitation events over ocean and over land.

1. Introduction

The impact of a rainfall event depends on how it unfolds as much as on the final rainfall tally. For example, 1.5 inches of rainfall in 24 hours in New York City may not have a significant negative effect. However, if the same rain falls within an hour in an intense downpour, it can cripple the subway system (http://cityroom.blogs.nytimes.com/2007/08/08/why-do-the-subways-flood/). Thus, knowledge of the statistics of rainfall and rainfall extremes at a wide range of timescales is highly desirable. Climate monitoring observations of global rainfall typically use daily rain gauge accumulation reports, but these observations have key limitations. First, the vast majority of gauges are on land (with the exception of a small number of buoys, e.g. *McPhaden et al.* 1998). Second, daily rain gauge reports provide only information on

---

M. Biasutti, Lamont-Doherty Earth Observatory of Columbia University. 61 Route 9W. Palisades, NY 10964-8000 (biasutti@ldeo.columbia.edu)

S.E. Yuter, Department of Marine, Earth, and Atmospheric Sciences. North Carolina State University

accumulation, not rainfall intensity or duration. As a consequence, most of the research on climate change and rainfall extremes is limited to the daily timescale—even though the expectation of more extreme precipitation under global warming comes from the link between atmospheric humidity and rainfall at the scale of convection (*Allen and Ingram* 2002; *Trenberth et al.* 2003). For example, *Alexander et al.* (2006); *Tebaldi et al.* (2006); *O'Gorman and Schneider* (2009) have looked at observed trends and projections for daily accumulation. Modeling studies that are relevant for trends in hourly precipitation rates are idealized (e.g., *Muller et al.* 2011) or focus on trends in the occurrence and severity of tropical cyclones and extra-tropical severe storms (e.g., *Vecchi and Soden* 2007; *Knutson et al.* 2010; *Trapp et al.* 2007). Observational studies of hourly precipitation trends are limited to a few stations in the mid latitudes (*Lenderink and Van Meijgaard* 2008; *Lenderink and van Meijgaard* 2010; *Shaw et al.* 2011).

For their part, meteorologists have traditionally looked at rainfall extremes in terms of individual intense storms. While isolated storms can produce heavy rainfall on scales of minutes, the majority of tropical rainfall is associated with mesoscale convective systems (MCS) or mesoscale convective complexes (MCC), and research has focused on explaining the conditions that make these storms possible. Moisture, lift, and instability must all be present for convective-type precipitation to occur (*Schultz and Schumacher* 1999). Forecasters usually look first for convective available potential energy (CAPE; the integrated positive buoyancy from the level of free convection to the equilibrium level) to determine if moisture and instability are present. Next, they look at convective inhibition (CIN; the work needed to lift the parcel to its level of free convection) and sources of lift to overcome CIN to determine if storms will develop. Finally, they look at vertical wind shear for information on how the convective storms will be organized (*Markowski and Richardson* 2010). *Laing and Fritsch* (2000) characterized the mean genesis environments for MCC as having locally strong values of both CAPE and low-level vertical wind shear. They found two primary situations where MCC often develop: (1) where the interaction of a moist-downdraft–generated cold pool and low-level vertical wind shear lifts a surface-based layer of high θ_e air (*Rotunno et al.* 1988; *Weisman* 1992) and (2) where a (typically nocturnal) low-level jet of high θ_e air overruns a frontal zone. Fronts being a mid-latitude phenomenon, the latter mechanism is not relevant within 15 ^{o} of the Equator.

A climatology of storm characteristics in the entire tropical band has been made possible with the collection of more than a decade of observations from the Tropical Rainfall Measuring Mission (TRMM). These data can provide a broader view on the conditions for intense precipitation events, clarify the relationship between the intensity of rainfall events and rainfall accumulation, and narrow the gap between the views of climatologists and meteorologists. For example, *Zipser et al.* (2006) used several measurements of cloud and hydrometeor characteristics to identify the geographical distribution of intense storms and weaker precipitation systems. In their conclusions, they noted a discrepancy between intense storms and heavy seasonal rainfall: “The strongest convective storms are often found in semiarid regions, while the heavy rains of the oceanic ITCZ, western Amazonia, and much of southeast Asia and Indonesia have relatively few intense storms. In parts of the Indian subcontinent, the most intense storms occur in the premonsoon months, while the rainiest parts of the monsoon consist of numerous weather systems but few severe storms” (*Zipser et al.* 2006).

These conclusions are supported by a number of other studies based on TRMM data that focus on selected regions and seasons. For example, *Schumacher and Houze* (2006) noted the lower intensity and higher frequency of rainfall events over the Atlantic compared with West Africa and also noted that the monsoon season is characterized by higher convective sustainability and lower shear, important factors for the production of stratiform rain. Similarly, *Kodama et al.* (2005) observed stronger convection and lightning activity during the pre-monsoon season in South America and India than during the monsoon season. More recently, *Romatschke et al.* (2010) noted that deep convective cores are characteristic of the pre-monsoon season of India and organized convective systems with large stratiform components are typical of the monsoon season. *Williams et al.* (2002) examined the seasonal evolution of thunderstorm activity in conjunction with environmental variations in CAPE and aerosols to understand if the latter can play a role in modulating lightning. Additionally, they indicated that, under certain conditions present in the western Amazon, the lines between maritime rains and continental showers (*Ramage* 1971) are blurred. *Liu* (2011) mapped several measures of precipitation-feature intensity (including echo top height, maximum height of 30 dBZ contour, and minimum 85 GHz TRMM Microwave Imager polarization-corrected brightness temperatures) and showed that the storms with largest graupel and hail, and thus strongest updrafts, occurred in Equatorial Africa and Argentina.

In *Biasutti et al.* (2011), we used surface reflectivity values from the TRMM Precipitation Radar (PR) to create a 10-year (1998-2007) monthly climatology of frequency of rain (f; the percentage of satellite snapshots in which rainfall is detected) and of mean conditional intensity (i; the mean rainfall calculated over rainy snapshots) at the original radar resolution of 0.05^o x 0.05^o. This dataset portrays the mean characteristics of precipitation events and thus is a variation of the TRMM-derived storm climatology of *Zipser et al.* (2006). Rainfall frequency, which is dominated by weak and moderate-intensity precipitation systems, is highest over the precipitation centers of the ocean (i.e., those with high monthly rain rates such as the Pacific and Atlantic Intertropical Convergence Zones (ITCZs), the Warm Pool, and the Bay of Bengal). Rainfall reaches similar peak frequencies over land only in the Amazon and over mountain ranges. Conditional intensity, on the other hand, clearly identifies regions with a propensity for very intense storms, such as the Himalayan Indentation (see also *Zipser et al.* 2006; *Romatschke et al.* 2010). However, in general, conditional intensity presents weaker and broader spatial variations than frequency. Intensities are often higher over land than ocean (as shown by multiple previous studies using measurements as different as lightning frequency and cloud top temperatures, e.g. *Zipser et al.* 2006; *Liu and Zipser* 2009). Peak intensity values are found in the subtropical latitudes of both North and South America, in the Congo Basin, and in the Himalayan indentation, while the Amazon has rainfall intensities between typical oceanic and continental values. The annual-mean and seasonal-mean patterns of frequency and conditional intensity presented in *Biasutti et al.* (2011) are consistent with previous literature on storm characteristics (e.g., *McCollum et al.* 2000; *Williams et al.* 2002; *Schumacher and Houze* 2003; *Romatschke and Houze* 2010; *Romatschke et al.* 2010), and the agreement indicates that this dataset can be used to investigate spatial and seasonal variations in storm characteristics across the tropics.

In this study, we use a tropic-wide dataset to systematically document estimated rainfall frequency, conditional intensity, and the relationship between them. We specifically focus on how the relationship between frequency and intensity changes seasonally and across a variety of rainfall regimes, from oceanic to continental and from humid to semi-arid. We then combine our gridded dataset with the precipitation feature dataset of the University of Utah Precipitation Measuring Mission (*Nesbitt et al.* 2000; *Liu et al.* 2008), which is organized by storm, to interpret our results in terms of storm characteristics, namely the prevalence of stratiform or convective rainfall. Finally, we investigate if the kind of data currently available from climate simulations, specifically the daily aggregated values of convective and large-scale (stratiform) rainfall, is sufficient to describe the rainfall events, or if additional model output is needed to compare model simulations and observations at the storm timescale.

This study complements previous work by authors at the University of Utah using their precipitation feature dataset (initially developed by *Nesbitt et al.* (2000) and further refined by *Liu et al.* (2008)), including *Toracinta et al.* (2002), *Nesbitt and Zipser* (2003); *Nesbitt et al.* (2004); *Cecil et al.* (2005); *Liu and Zipser* (2005); *Nesbitt et al.* (2006); *Zipser et al.* (2006); *Liu and Zipser* (2008, 2009). The focus of the current paper is on an aspect of global precipitation that was not fully addressed in previous work: the relationship between precipitation frequency and conditional intensity and how this relationship changes geographically and seasonally. We emphasize a comparison of climatological variations in storm intensity obtained from instantaneous rainfall measurements to climatological variations in mean daily accumulation on rainy days, a more common measure of rainfall intensity in climate studies. *Dai* (2001) examined global precipitation frequency using weather reports from the Comprehensive Ocean-Atmosphere Data Set (COADS) and inferred seasonal mean intensity by dividing the *Xie and Arkin* (1997) infrared-based seasonal precipitation estimates by seasonal frequency. In contrast, this study uses TRMM PR data for both frequency of precipitation and conditional rain rate (intensity), the latter of which is a better proxy for rain rates within individual storms than seasonal mean intensity.

Section 2 introduces the datasets used in this study and defines the relationship between our snapshot–based definition of frequency and intensity to the comparable variables obtained from daily aggregated data, namely the frequency of rainy days and the mean daily accumulated rainfall on rainy days. Section 3 describes our methodology using the central India region as an example. For this region, we analyze both instantaneous and daily frequency and intensity, and we describe how instantaneous conditional intensity peaks before frequency during the pre-monsoon seasons. In addition, we explain this result in terms of predominantly convective rainfall before the monsoon onset. Section 4 generalizes our findings for most of the tropical land masses, both those that experience a dry season and those that are quite rainy throughout the year. We also highlight the contrast between land and oceanic regions. The regions focused on in this study are shown in Figure 1. Section 5 discusses if current model output is sufficient to characterize mean storm intensity. Section 6 offers our summary and conclusions.

2. Data and Methods

a. Data sets

The TRMM PR (*Kummerow et al.* 2000) provides a unique opportunity to observe the climatology of rainfall in great detail with the same instrument over tropical land and ocean locations. Coverage extends to about 36^oN/S, and sampling of the diurnal cycle is quite uniform (*Negri et al.* 2002; *Hirose and Nakamura* 2005). We use a 1998-2007 monthly climatology (*Biasutti et al.* 2011) obtained by (1) binning the TRMM PR data from each individual swath onto a regular grid with spacing of 0.05^o in both longitude and latitude (about a 5 km grid) and (2) averaging the gridded data over the entire record to produce monthly climatologies. A minimum of about 1700 observations per gridpoint (up to a maximum of over 8000) are used.

Rainfall frequency at any location is defined as the number of observations in which a radar reflectivity Z is detected to be above the threshold of 18 dBZ, normalized by the total number of observations. This sensitivity threshold implies that drizzle events are not captured by the TRMM PR. As a measure of conditional rainfall intensity, we use the mean reflectivity when rain is detected (i.e., the averaging does not include dry states). Note that while the TRMM PR data also provide rainfall rates, there is some uncertainty in the rain/reflectivity (R/Z) conversion (see for example *Shige et al.* 2006). To bypass this issue, we conduct our analysis using mostly the attenuation-corrected reflectivity. However, rainfall values are used to show that our results are robust to the choice of intensity measure and as an intermediate step in our comparison with daily data. For this analysis, as with the station data described below, a rain event is one with instantaneous rain rates $>$0.4 mm hr^{-1}. When using reflectivity, averaging is performed on the reflectivity Z itself (mm^6 m^{-3}), and the conversion to dBZ is applied as the last step of the calculation. The near-linear relationship between rainfall and reflectivity allows us to loosely interpret mean reflectivity as mean rainfall intensity. We will refer to the conditional reflectivity as intensity.

Frequency and intensity (f and i) from the TRMM PR data are compared to their daily counterparts obtained from TRMM 3B42 (*Huffman et al.* 2007): the number of rainy days with $\geq$1 mm of accumulation (R1) and the simple daily intensity index (SDII), which is the mean accumulation on rainy days. TRMM 3B42 data are obtained by merging information from the TRMM instruments with infrared and visible sensors on geostationary satellites. The TRMM 3B42 product is gridded at 0.25^o resolution.

Using station data, we confirm that differences between the patterns of TRMM PR f and i on one hand and TRMM 3B42 R1 and SDII on the other can result from temporal aggregation, as opposed to resulting from spatial averaging only. As an example, we use the minute-by-minute gauge observations of rainfall at the U.S. Department of Energy Atmospheric Radiation Measurement (ARM) Climate Research Facility site in Darwin, Australia. (Rainfall time series taken from other ARM sites paint the same picture, not shown.) Although there are differences between the instantaneous rainfall estimates obtained from different instruments, the description of the role of temporal aggregation on frequency and intensity time series is independent of the instrumentation as long as the instrument is appropriate for high-frequency sampling. We use values from the optical rain gauge.

We focus on a subset of parameters from the *Liu et al.* (2008) precipitation feature database. We examine the following variables of each precipitation feature from the orbit-by-orbit Level 2 data: (1) number of pixels with stratiform rain, (2) number of pixels with convective rainfall, (3) stratiform volumetric rain (km^2 mm hr^{-1}), and (3) convective volumetric rain (km^2 mm hr^{-1}). The number of pixels multiplied by 25 km^2 is the area covered by the precipitation feature. We also use Level 3 data from the same precipitation feature database, specifically monthly total convective and stratiform rainfall.

We use ERA-Interim estimates of daily convective and stratiform rainfall (Sec. 5). *Dee et al.* (2011) documented the use of observations in producing the reanalysis and assessed the remaining biases.

We also use annual mean rainfall rates from *Huffman et al.* (1997).

b. The effect of temporal aggregation on frequency and intensity time series

Figure 2 shows the annual mean frequency and intensity of rainfall events (f and i) as estimated from the snapshot data of the TRMM PR and the frequency and intensity of rainy days (R1 and SDII) estimated from TRMM 3B42. The annual mean rate rates estimated from GPCP are superimposed. As noted in more detail in *Biasutti et al.* (2011), variations in intensity i are broad in scale, while frequency f shows sharp gradients at all scales. The two patterns have little in common other than the fact that places with no rain appear in both fields. Most variations in annual mean rain rates are captured by variations in f. Similarly, the R1 field is more closely related to overall rain rates than the SDII field (Figure 2c,d), yet we see that the distinctions in patterns between the two fields has faded compared with the snapshot-based fields. For example, the maximum rainfall rates in the ITCZs, the Southern Pacific Convergence Zone (SPCZ), and the southern Indian Ocean are visible in the SDII field, and the maximum rainfall along the coast of Myanmar is ascribed to a maximum in SDII and not in R1. The opposite is true for TRMM PR data where higher frequency of rain events is clearly linked to the large rain rates with intensity gradients playing no role. Another clear example of the difference is the Congo Basin. Although this is a region with explosive storms and some of the highest i values in the tropical band, it appears in the SDII map as a region of modest daily intensity.

We can ensure that the observed difference between TRMM products is indeed a consequence of the temporal aggregation, rather than the spatial aggregation or the method of precipitation estimation in the two retrievals, by comparing f and i with R1 and SDII for gauge measurements. As an example, we present measurements from Darwin, Australia, over the course of 1 rainy season (2010-2011). Fig. 3 shows the seasonal evolution of 10-day (dekad) averages of rain frequency and intensity defined from data at increasing temporal aggregation. In the first panel, we use optical rain gauge data at 1 minute resolution. In the second panel, we have aggregated rainfall data at hourly resolution and calculate the 10-day average frequency and intensity using the same definition of rainy event (rain rates $>$0.4 mm hr^{-1}) as for minute-by-minute data. In the third panel, we plot R1 and SDII. As the temporal aggregation increases, frequency values increase and intensity values decrease. This result is dependent both on the episodic nature of rainfall in Darwin and on the thresholds that define a rain event or a rainy day. Across the three panels of Fig. 3, the relationship between dekadal mean frequency and intensity of rainfall changes, in consequence to the fact the two quantities are defined from rainfall measurements aggregated at increasingly longer times. The changing relationship is exemplified by the way in which events that appear as maxima in frequency when the latter is defined from minute-average data (Fig. 3a) appear as maxima in daily intensity (Fig. 3c). These same events appear as local maxima in both frequency and intensity defined at the intermediate hourly timescales (Fig. 3b). One example of this is the large storm to hit Darwin in mid-February 2011, which is visible in the 17th dekadal average. The 1-min averaged data show it was raining 32% of time during the10-day period with a conditional rainfall intensity of 11 mm/hr. The R1 value for the same10-day period indicates that it rained more than 1 mm on 8 out of the

10 days (80%) with SDII (average accumulation) of 4 mm/day. More generally, we note that the correlation between dekadal frequency and intensity increases dramatically going from rainfall data aggregated at the minute to daily timescale. This increase in correlation was also apparent in the map view of Fig. 2: The SDII pattern matches the R1 pattern (in the ITCZs, for example) better than the i pattern matches the f pattern.

3. Seasonal variations of rainfall intensity in India

We have noted above that the snapshot definition of frequency and intensity paints a complex picture of tropical rainfall. On one hand, it highlights the role of rainfall frequency in determining rain rates for a single storm (as seen for Darwin in Fig. 3) or in setting the spatial gradients in annual mean rainfall (Fig. 2). On the other hand, it highlights the tendency for relatively dry places to have more intense rain than places with more frequent rain, be it land compared to ocean or the Congo compared to the Amazon. In the reminder of this paper, we explore the relationship between rainfall frequency and intensity in the context of the seasonal cycle and show that (1) there is no universal relationship between mean frequency and mean intensity at any given location and (2) mean intensity over most tropical land areas is largest just before the core of the rainy season when frequency becomes largest. We further interpret the latter result in terms of the larger amount of stratiform precipitation relative to convective precipitation in the rainy season. In this section, we focus on a region in central India, which permits us to present our methodology in more detail and to compare our results to an additional dataset based on gauge measurements of daily rainfall. In the following section, we will extend our analysis of f and i to other areas.

In Fig. 4, we show the Hoevmoeller diagram of rainfall frequency and intensity averaged over land points over the longitudes 78^{o}E to 83^{o}E. The panels on the left are for f and i derived from the TRMM PR data; the panels in the center and on the right are for R1 and SDII derived from daily data from TRMM 3B42 and from the gridded product of the Indian Meteorological Department (IMD), respectively. The inception of the monsoon is characterized by an increase in frequency of rain events and frequency of rainy days (i. e., both f and R1) that occur at the same time for all latitudes considered here (10^{o}N to 26^{o}N). The mean daily intensity also goes up during the monsoon season in both TRMM3B42 and IMD (Fig. 4b,c): It is at a minimum in May and at a maximum in July and August. After that, it decays slowly: October values are still larger than May values. There are differences between the satellite-based and the ground-based datasets, such as the strength of the maximum of both R1 and SDII in the northern part of the domain, but these differences do not detract from this consistent picture. The PR data (Fig. 4a) tell a different story: Conditional intensity (i) is at a maximum well before the onset of monsoon season, and it is actually at a relative minimum at the core of the rainy season. During the retreat of the monsoon in October, the PR data show average intensities comparable to those at the onset in June but lower than the spring values. To make the comparison with the daily-based data more straightforward, we have contoured rainfall intensity in mm hr^{-1} on top of the dBZ field. The close correspondence that the two measures of intensity indicates that they are interchangeable for our purposes.

We can look further into this data and contrast the joint probability density functions (JPDFs) of frequency and intensity during the core monsoon months and in the prior season (Fig. 5). When we use PR data (Fig 5a,b), each gridpoint provides one entry in the distribution for each season, meaning that climatological May-June average f and i at each gridpoint in central India contribute to the JPDF of the pre-onset season and climatological July-August-September averages enter the monsoon-season JPDF. The region chosen (17^oN to 25^oN, 78^oE to 83^oE) has no defined gradients in either frequency or intensity, and therefore the JPDFs describe general characteristics of the area. We compare the JPDFs obtained from TRMM PR data with two definitions of intensity (one using reflectivity and one using rain rates) to the JPDFs obtained from the daily TRMM 3B42 data. In this case each datapoint comes from a different gridpoint and a different year. There is a substantial overlap between the two seasonal distributions, especially in the PR case, in part due to the fact that we chose May-June as representative of pre-onset conditions even though the Indian monsoon often starts in the middle of June. However, it is clear that the monsoon season is characterized by higher frequency of rainfall events and rainy days. Moreover, the PR data indicate that the pre-monsoon season has a higher mean value of conditional intensity than the monsoon season. This finding is true for all frequencies at which both distributions exist and should therefore be considered a robust, although small, difference. The PR data also show a wider JPDF during May-June, which indicates that mean conditional intensity varies more widely across gridpoints in the pre-monsoon season. Instead, the daily data depict the transition from pre-monsoon to monsoon as a simple shift of the JPDF toward both higher frequency and higher intensity, which is consistent with Fig. 4. We also note that in the PR dataset average summer values of conditional intensity are nearly independent of frequency—except at very low frequency. As noted in the introduction, contrasting patterns of frequency and intensity could suggest that higher intensity and smaller frequencies are related. However, a negative relationship is inconsistent with the summer JPDF for India (or other locations, as will be explained in the next section). This finding indicates that explanations for the spatial patterns of f and i will have to be specific to place and time and cannot rely on a general relationship between the two quantities.

To understand more thoroughly why the pre-monsoon season has a wider range of intensities and a higher overall mean intensity, we take advantage of a different dataset produced from the TRMM PR: the precipitation feature dataset of *Nesbitt et al.* (2000) and *Liu et al.* (2008). For all rainfall events, this dataset provides, among many other parameters, a distinction between convective and stratiform rain amounts and areas (*Houze* 1993; *Steiner et al.* 1995). We selected all the events happening in the central India region during May-June and July-August for the same 10 years on which our climatology is based and compared the relative importance of stratiform and convective rainfall in the two seasons. This analysis is summarized in Fig. 6. Fig. 6a and Fig. 6b contrast the seasonal evolution of rainfall area and rainfall amounts for both convective and stratiform rainfall. July-August totals are larger than May-June in all counts (convective or stratiform; area or amount). The seasonal evolution of rainfall frequency can be traced as the seasonal evolution of total stratiform area (Fig. 6a) because of both the areal extension and the duration of stratiform precipitation. The seasonal evolution of conditional intensity can be explained in terms of the balance between stratiform and convective rain per storm (Fig. 6c,d,f). The pre-onset months differ from the rainy season months because, on average, spring storms have less area experiencing stratiform rain and more area experiencing convective rain. This means it is more likely that a rain event is convective. The ratio of convective to stratiform area is only about 0.2 during the core of the rainy season, but it more than triples to 0.7 during April and May (Fig. 6f). Thus, spring conditional intensities are higher because the low-intensity stratiform rain is less likely to factor into the averaging. Note that when we look at rainfall rates per pixel (Fig. 6e), the intensity of convective rain is similar in the pre-onset months and core rainy season months, whereas the intensity of stratiform rain actually increases in the rainy season. The higher values of conditional intensity seen in Fig. 5 during spring result from the lack of stratiform rain in the samples and not from more explosive convective cells. Similarly, the higher ratio of convective to stratiform rainfall explains the higher variability in conditional intensity in spring because stratiform rain spans a much narrower range of possible intensities than convective rain does (Fig. 6e and *Steiner et al.* 1995).

4. The relationship between frequency and intensity of rainfall over tropical regions

The purpose of this section is to show that in all tropical land regions the months before the core rainy season are characterized by a relative prominence of convective rainfall and thus by conditional intensities that are spatially more variable and higher in the mean. First, we survey land regions with seasonal cycles that are fundamentally different from that of India, and then we repeat our analysis on oceanic regions to draw the contrast between continental and maritime environments.

a. Other monsoon regions

We first focus on two monsoon regions (West Africa and Australia) that differ from India because of their proximity to deserts and the presence of a more complex circulation with a shallow thermal cell superimposed on the deep monsoonal circulation. Similar analysis for the monsoon regions of South America and South Africa (Fig. 1) produces the same main result of maximum intensity during the pre-onset months. Fig. 7 shows the seasonal evolution of rainfall frequency and rainfall intensity averaged over the longitudes of West Africa (5^oW to 5^oE) and central Australia (130^oE to 135^oE). In both places, we clearly see the seasonal migration of rainfall, which expands from the ocean to land during the summer season. As before, we see that the rainy season is characterized by more frequent rainfall events. In addition, the onset of the rainy season over land is preceded by a maximum in conditional intensity. This is especially apparent for the Australian region: The land portion of the domain (south of 12^oS) sees maximum intensities during October-November-December. In contrast, the ocean region immediately to the north sees a smooth transition between the low values of the dry season to a very broad maximum extending from October to July.

The thick line superimposed on the frequency and intensity fields is the confluence line, the contour of zero meridional wind at the surface. It has long been noted (see for example the reference to colonial scientists in Africa in the early 20th century in *Hastenrath* 1991) that the rain band in these monsoon areas is distinct from the ITCZ. The ITCZ is defined by surface convergence and is closely related to the meridional confluence line (see also *Nicholson* (2009)). In the mean, the confluence line represents the edge of a shallow direct circulation (*Zhang et al.* 2006). The deep convection that makes up the rain band is found further equatorward where temperature and humidity combine to give higher values of boundary-layer equivalent potential temperature (*Nie et al.* 2010). However, the correspondence between the confluence line and a sharp gradient in conditional intensity over land indicates that the mean misses some subtleties: Albeit rarely, deep convection sometimes occurs as far north as the monsoon flow can reach—but no further. The role of the confluence line as a boundary for deep convection is clear in both West Africa and Australia. In Australia, the effect is most visible in the pre-onset months and becomes less visible as the monsoon retreats. This difference could be due to the fact that the Australian monsoon is not captured as well by a simple zonal mean circulation. Alternatively, we speculate that it might be indicative of a real difference in the effectiveness of dry advection in capping deep convection at the beginning of the season, when the land is dry, compared with the end of the season, when the land is moist.

Figures 8 and 9 provide a more quantitative assessment of the difference in conditional intensity between the pre-onset and rainy season months. The JPDFs of frequency and intensity confirm that the pre-onset months in both regions have higher mean values of conditional intensity and more spatial variability, which is similar to central India (albeit, the differences are smaller). The analysis of the precipitation features summarized in Fig. 9 confirms that, as seen over India, the core of the rainy season is characterized by events that have smaller convective area and larger stratiform area. The area of convective rainfall relative to that of stratiform rainfall is reduced from pre-onset months to core rainy season by a factor of nearly 2 and 3 in West Africa and Australia, respectively. The rainfall rates per pixel behave differently in different regions: They tend to become higher as the season progresses in Africa, but they are highest in the pre-onset months in Australia. The fact that convective rainfall rates per pixel do not exhibit a consistent seasonal evolution across the monsoon regions, but conditional intensity does, supports the idea that the dominant mechanism for higher conditional intensities during the pre-onset months is the prevalent sampling of convective rainfall.

In monsoon regions, the retreat of the rains defines a season comparable to the onset season, but we do not observe a comparable peak in conditional intensity. The asymmetry is especially apparent in Australia, but the reason is unclear.

b. Equatorial land regions

We complete our survey of tropical land regions by examining South America and central Africa. Our focus is on the equatorial portion of the regions, where some amount of rainfall is present year round.

Fig. 10 shows the seasonal evolution of rainfall frequency and intensity. There are notable differences in the annual cycle of rainfall in the two regions: Rainfall frequency over the Congo has a strong semi-annual component, whereas the Amazon has one strong annual peak in March-April-May. The Congo presents the same relationship between frequency and intensity seen in monsoon regions: peak intensity precedes peak frequency. In South America, we clearly see a maximum in intensity values from August to October when frequency is minimum and consistent with the other regions. However, the region north of the Equator does not behave as expected. During December-January-February, both frequency and intensity experience a relative minimum. As shown below, this behavior is typical of ocean regions. The analysis of the precipitation features (Fig. 11) reveals that the intensity peak is due to a maximum in convective area in the Amazon where the relative area of convective to stratiform goes from 0.2 to 0.6 between April and September. This maximum in convective area also occurs in the Congo during June-July-August. The fraction of convective area in the Congo is 0.5 in July and approximately 0.3 in March and October. The January-February-March peak in the Congo is due in part to larger convective areas but mostly due to higher convective intensities.

c. Oceanic regions

Frequency and conditional intensity over oceanic regions follow a different pattern than what is observed over continental regions. Here we present two examples: (1) the central Pacific at the eastern edge of the warm pool, where the ITCZ and the SPCZ merge and rainfall is widespread in the whole domain, and (2) the eastern Pacific, where rainfall is dominated by a well-defined ITCZ north of the Equator and a secondary rainfall maximum south of the Equator during boreal spring. The Hoevmoeller diagram of rainfall frequency and intensity is presented in Fig. 12. As we would expect from climatological rain rates, rainfall frequency is highest in the ITCZ in the eastern Pacific and mostly uniform in the central Pacific. Over these oceanic regions, variations in intensity mimic frequency to a large degree. This finding, which is very apparent in the ITCZ of the eastern Pacific, is less apparent in the central Pacific, where the patterns of frequency and intensity are not sharply defined. Unlike continental regions, there is no indication that intensity is higher outside the area of maximum frequency in either the eastern or the central Pacific (or the Atlantic ITCZ; not shown). This implies that the intensity pattern is similar at daily and individual storm timescales. The overall homogeneity of rainfall intensity is confirmed by Fig. 13, which shows seasonal variations in storm convective and stratiform area and rain rates. The fraction of convective area relative to stratiform area is minimum when frequency is maximum, as expected, but the seasonal range is trivial in both regions, with the ratio going from 0.15 to 0.25 in the eastern Pacific and staying around 0.25 in the central Pacific. The seasonal changes in convective rain rates parallel those of frequency (see for example the maximum in the eastern Pacific during northern fall) and are the dominant effect.

5. Can current model output characterize rain events?

The above analysis has shown that we can learn a great deal about the nature of storms from instantaneous rainfall data: (1) Ocean regions have more-frequent and less-intense storms than land regions, with little seasonality or spatial gradients in the characteristics of the storms; (2) land regions have considerable variations in storm intensity seasonally and especially spatially (contrast, for example, the Congo and the Amazon or the southwest and southeast United States); and (3) storms in any given land region are more intense during the development than during the core of the rainy season. We now turn our attention to determining if the kind of aggregated rainfall data that is typically output from climate models is sufficient to characterize what kind of storms occurs in any given region in any given season.

Previous sections have shown that the preponderance of stratiform or convective rainfall can explain the contrast in rainfall characteristics between land and ocean, as well as seasonal variations over a selected region. Climate models do not explicitly simulate convection, but they do parametrize it, and they distinguish between convective and stratiform (or large-scale) precipitation. Although climate simulations do not output instantaneous values of precipitation, they often do output accumulation of convective and stratiform components at daily and longer timescales. We can, therefore, investigate whether daily values of convective and stratiform precipitation can properly describe storm characteristics across regions and seasons. Our goal is not to assess model biases in the kind of rain events produced but instead to identify if such biases can be detected. Thus, we continue to look at observations, but aggregated in a way comparable to what is available for climate models.

Figure 14 shows the annual mean ratio of convective to stratiform rainfall calculated from TRMM L3 (Level 3 products of the University of Utah Precipitation Measuring Mission dataset) and from ERA-Interim reanalysis. In the case of TRMM L3, the ratio is calculated from monthly total convective and stratiform rainfall data and then averaged over 120 months (1998-2007). Months with minimal rainfall are masked out so the stratus decks and desert regions appear as missing data. (Note that TRMM does not detect drizzle in stratocumulus.) In the case of the reanalysis, the daily values of convective and stratiform rain are used to calculate the daily ratio, which is then averaged over the same 10 years. ERA-Interim rainfall rates are model output, but they are constrained by the assimilation of radiances. There are large difference across the two estimates that are probably due to model bias combined with measurement deficiencies and averaging choices. These differences are beyond the scope of our discussion. (The performance of the reanalysis is addressed in *Dee et al.* 2011). What interests us is that both estimates capture some features of the instantaneous intensity pattern shown in Figure 2b but not its overall pattern. For example, local maxima in the Himalayan Indentation and in the Sahel are captured by both the convective ratio (as calculated from these aggregated rainfall data) and the intensity. However, the convective ratio does not adequately capture the broad difference in intensity between land and ocean or between the ITCZ regions and oceanic regions nearby, and it does not adequately capture the extreme intensities in the Congo and the American

Plains. If we consider the TRMM data, which is free of model biases, we can ascribe the discrepancies between instantaneous intensity (Figure 2b) and monthly convective fraction (Figure 14a) to the fact that rainfall data have been aggregated in time. This assertion is proved by comparing our estimates of convective ratio to the estimate provided by *Schumacher and Houze* (2003), which was calculated from instantaneous data and which clearly highlights high convective ratios in those regions where we see high instantaneous intensity. (Note that Fig. 3 in *Schumacher and Houze* (2003) shows stratiform ratio, which is the complement to convective ratio. Thus, a minimum in one is a maximum in the other.)

Despite its previously discussed limitations, the aggregated convective ratio can still convey useful information about the spatial distribution of and seasonal changes in storm intensity. To show this, we present regional averages of convective and stratiform daily rainfall estimated from ERA-Interim (Fig. 15). As mentioned before, both daily convective and stratiform rainfall rates are highest at the peak of the rainy season because daily rain rates integrate values of instantaneous rain rates and rain frequency. At the same time, the daily convective ratio matches instantaneous observations in two important ways: (1) It declines during the core of the rainy seasons in each region, and (2) it shows a seasonal range that is largest in monsoon regions, reduced over other continental lands, and negligible over the oceans. These distinctions suggest that this measure of convective ratio captures—at least qualitatively—some of the spatial differences and seasonality of storm characteristics.

We conclude that the ratio of convective to stratiform rainfall, even when aggregated at daily timescales, is useful to monitor the seasonal changes in storm intensity in a variety of environments. However, it is not sufficient to distinguish the mean storm intensity in different regions. To do so, it is necessary to consider conditional intensity at much higher temporal resolution.

6. Summary and Conclusion

The need for a better description of the range and controls of rainfall intensity at hourly or shorter timescales is acute. This is particularly true for the tropics, where some very intense storms occur and the infrastructure of cities and agriculture alike is extremely vulnerable.

The TRMM PR has taken snapshots of the 3-dimensional structure of rainfall events since 1998, providing a unique insight into the nature of tropical rainfall. We use two datasets derived from this instrument to assess the seasonal variations of rainfall intensity at the scale of individual rain events and to determine the associated variations in storm structure. The first dataset (*Biasutti et al.* 2011) is a gridded monthly climatology of the frequency and conditional intensity of rainfall events. The second dataset (*Liu et al.* 2008) is organized by storm and is used in this work to determine the relative contribution of stratiform to convective rainfall in each event.

On average, the highest rainfall intensities occur over land and have a distinct seasonality. Over most tropical land, peak rainfall accumulation does not occur at the same time as peak rainfall intensity. Instead, the months preceding the core of the rainy season, when frequency of rainfall is still low, show the highest conditional intensity. This high intensity is due to a high prevalence of convective precipitation areas and fewer developed stratiform precipitation areas. The total convective area increases during the rainy season; however, stratiform areas grow more and become dominant, so the average rainfall intensity declines as frequency of rainfall increases. While previous studies have addressed these points regionally (see for example *Zipser et al.* 2006, and further examples discussed in the introduction), we present a tropic-wide systematic survey and show that variations in precipitation structures between the development phase and the core of the rainy season are nearly consistent in different geographic regions (i.e., in the monsoon regions of India, West Africa, Australia, South America, South Africa, and in equatorial land regions). Over the ocean, the highest intensity coincides with highest rain frequency and thus highest rain accumulation. Here, the convective precipitation rain rates are higher at times of more frequent rainfall and variations in the ratio of convective to stratiform area are too small to fully compensate for this effect.

The climate community's work on extreme precipitation in the Tropics has focused primarily on tropical cyclones or on the highest percentiles of daily rainfall accumulation, and has often been limited to oceanic regions. Our observational analysis indicates that these limitations are problematic. First, we have illustrated that daily accumulations are not sufficient to capture the occurrence of individual intense storms because high accumulations can result from a short period of high-intensity rainfall, a higher frequency of lower-intensity rainfall, or some combination of the two. For example, we have shown that neither the SDII nor the convective ratio calculated from daily aggregated data provide any indication of the occurrence of very intense storms over the Congo. The daily timescale is relevant for certain impacts, but it is important to consider that high daily intensity and high storm intensity do not typically coincide. Second, we have shown that seasonal variations in the ratio of stratiform to convective rainfall are large over land and small over ocean. The marked seasonality in storms characteristics over land is in sharp contrast to the relative homogeneity of oceanic storms. Thus, when trying to understand how a changing climate will affect extreme precipitation, we should be mindful that scalings that are valid over the oceans may not be pertinent to extremes over land.

Finally, we have shown that some aspects of the seasonal variations in precipitation structure over land can be validated with current climate model outputs—namely, the daily convective and stratiform rainfall accumulation. However, to better differentiate storms (for example, between those characteristic of the Congo versus the Amazon), it is necessary to first calculate the instantaneous rainfall intensity and convective rainfall ratio at each model time step and then output their daily averages. Given the importance of understanding how extreme precipitation will change over land regions— including at the timescale of individual storms—we suggest that these quantities also be saved as routine output by climate models.

Acknowledgments. ECMWF ERA-Interim data used in this study have been provided by ECMWF (http://data-portal.ecmwf.int/). The precipitation feature dataset was obtained from the University of Utah Precipitation Measuring Mission pages (http://trmm.chpc.utah.edu/). The TRMM 3B42 data were obtained from the IRI data library (http://iridl.ldeo.columbia.edu/). The Indian Meteorology Department data were obtained through Erika Coppola of the International Center for Theoretical Physics.

This work was supported by NASA grant NNX07AD21G and NSF grants ATM-0544766 and ATM-0908420. Any opinions, findings, and conclusions or recommendations expressed in this material are those of the authors and do not necessarily reflect the views of NASA or NSF.

REFERENCES

Alexander, L., et al., Global observed changes in daily climate extremes of temperature and precipitation, *Journal of Geophysical Research*, *111*(D5), 5109, doi:DOI:10.1029/2005JD006290, 2006.

Allen, M. R., and W. J. Ingram, Constraints on future changes in climate and the hydrologic cycle , *Nature*, *419*, 224–232, 2002.

Biasutti, M., A. H. Sobel, S. J. Camarago, and T. T. Creyts, Projected changes in the physical climate of the Gulf Coast and Caribbean, *Climatic Change*, doi:10.1007/s10584-011-0254-y, 10.1007/s10584-011-0254-y, 2011.

Cecil, D. J., S. J. Goodman, D. J. Boccippio, E. J. Zipser, and S. W. Nesbitt, Three Years of TRMM Precipitation Features. Part I: Radar, Radiometric, and Lightning Characteristics, *Monthly Weather Review*, *133*(3), 543–566, 2005.

Dai, A., Global precipitation and thunderstorm frequencies. Part I: Seasonal and interannual variations, *Journal of Climate*, 2001.

Dee, D. P., et al., The ERA-Interim reanalysis: configuration and performance of the data assimilation system, *Quarterly Journal of the Royal Meteorological Society*, *137*(656), 553–597, 2011.

Hastenrath, S., *Climate dynamics of the Tropics*, Kluwer Academic Publishers- Dordrecht, The Netherlands, 1991.

Hirose, M., and K. Nakamura, Spatial and diurnal variation of precipitation systems over Asia observed by the TRMM Precipitation Radar, *Journal of Geophysical Research*, *110*(D5), D05,106, doi:doi:10.1029/2004JD004815, 2005.

Houze, R. A., Jr., *Cloud Dynamics*, Academic Press, 1993.

Huffman, G., D. Bolvin, E. Nelkin, D. Wolff, R. Adler, G. Gu, Y. Hong, K. Bowman, and E. Stocker, The TRMM Multisatellite Precipitation Analysis (TMPA): Quasi-global, multiyear, combined-sensor precipitation estimates at fine scales, *Journal of Hydrometeorology*, *8*(1), 38–55, doi:10.1175/JHM560.1, 2007.

Huffman, G. J., et al., The Global Precipitation Climatology Project (GPCP) Combined Precipitation Data Set., *Bull. Amer. Meteor. Soc.*, *78*, 5–20, 1997.

Knutson, T. R., et al., Tropical cyclones and climate change, *Nature Geoscience*, *3*(3), 157–163, 2010.

Kodama, Y.-M., A. Ohta, M. Katsumata, S. Mori, S. Satoh, and H. Ueda, Seasonal transition of predominant precipitation type and lightning activity over tropical monsoon areas derived from TRMM observations, *Geophysical Research Letters*, *32*(14), L14,710–, 2005.

Kummerow, C., et al., The status of the Tropical Rainfall Measuring Mission (TRMM) after two years in orbit, *Journal of Applied Meteorology*, *39*(12), 1965–1982, 2000.

Laing, A. G., and J. M. Fritsch, The large-scale environments of the global populations of mesoscale convective complexes, *Monthly Weather Review*, *128*(8), 2756–2776, 2000.

Lenderink, G., and E. Van Meijgaard, Increase in hourly precipitation extremes beyond expectations from temperature changes, *Nature Geoscience*, *1*(8), 511–514, 2008.

Lenderink, G., and E. van Meijgaard, Linking increases in hourly precipitation extremes to atmospheric temperature and moisture changes, *Environmental Research Letters*, *5*(2), –, 2010.

Liu, C., Rainfall Contributions from Precipitation Systems with Different Sizes, Convective Intensities, and Durations over the Tropics and Subtropics, *Journal of Hydrometeo-*

rology, *12*(3), 394–412, 2011.

Liu, C., and E. J. Zipser, Global distribution of convection penetrating the tropical tropopause, *Journal of Geophysical Research*, *110*(D23), 2005.

Liu, C., and E. J. Zipser, Diurnal cycles of precipitation, clouds, and lightning in the tropics from 9 years of TRMM observations, *Geophysical Research Letters*, *35*(4), doi: doi:10.1029/2007GL032437, doi:10.1029/2007GL032437, 2008.

Liu, C., and E. J. Zipser, "Warm Rain" in the Tropics: Seasonal and regional distributions based on 9 yr of trmm data, *Journal of Climate*, *22*(3), 767–779, doi: 10.1175/2008JCLI2641.1, 2009.

Liu, C., E. J. Zipser, D. J. Cecil, S. W. Nesbitt, and S. Sherwood, A Cloud and Precipitation Feature Database from Nine Years of TRMM Observations, *Journal of Applied Meteorology and Climatology*, *47*(10), 2712–2728, 2008.

Markowski, P., and Y. Richardson, *Mesoscale meteorology in midlatitudes*, *Advances in Weather and Climate*, vol. 2, Wiley-Blackwell, 2010.

McCollum, J. R., A. Gruber, and M. B. Ba, Discrepancy between gauges and satellite estimates of rainfall in equatorial Africa, *Journal of Applied Meteorology*, *39*(5), 666–679, 2000.

McPhaden, M. J., et al., The Tropical Ocean-Global Atmosphere observing system: A decade of progress, *Journal of Geophysical Research*, *103*(C7), 14,169, 1998.

Muller, C. J., P. A. O'Gorman, and L. E. Back, Intensification of Precipitation Extremes with Warming in a Cloud-Resolving Model, *Journal of Climate*, *24*(11), 2784–2800, 2011.

Negri, A., T. Bell, and L. Xu, Sampling of the Diurnal Cycle of Precipitation Using TRMM, *Journal of Atmospheric and Oceanic Technology*, *19*(9), 1333–1344, 2002.

Nesbitt, S., and E. Zipser, The Diurnal Cycle of Rainfall and Convective Intensity according to Three Years of TRMM Measurements., *Journal of Climate*, *16*, 1456–1475, 2003.

Nesbitt, S., E. Zipser, and D. Cecil, A census of precipitation features in the Tropics using TRMM: Radar, ice scattering, and lightning observations, *Journal of Climate*, *13*(23), 4087–4106, 2000.

Nesbitt, S., E. Zipser, and C. D. Kummerow, An examination of version-5 rainfall estimates from the TRMM Microwave Imager, Precipitation Radar, and rain gauges on global, regional, and storm scales, *Journal of Applied Meteorology*, *43*(7), 1016–1036, 2004.

Nesbitt, S. W., R. Cifelli, and S. A. Rutledge, Storm Morphology and Rainfall Characteristics of TRMM Precipitation Features, *Monthly Weather Review*, *134*(10), 2702–2721, 2006.

Nicholson, S. E., A revised picture of the structure of the "monsoon" and land ITCZ over West Africa, *Climate Dynamics*, *32*(7-8), 1155–1171, 2009.

Nie, J., W. R. Boos, and Z. Kuang, Observational Evaluation of a Convective Quasi-Equilibrium View of Monsoons, *J Climate*, *23*(16), 4416–4428, 2010.

O'Gorman, P., and T. Schneider, The physical basis for increases in precipitation extremes in simulations of 21st-century climate change, *Proceedings of the National Academy of Sciences*, *106*(35), 14,773, doi:doi:10.1073/pnas.0907610106, 2009.

Ramage, C. S., *Monsoon metereology*, no. 15 in International Geophysics Series, Academic Press, 1971.

Romatschke, U., and R. A. Houze, Jr., Extreme summer convection in south america, *Journal of Climate*, *23*(14), 3761–3791, doi:10.1175/2010JCLI3465.1, 2010.

Romatschke, U., S. Medina, and R. A. Houze, Jr., Regional, seasonal, and diurnal variations of extreme convection in the South Asian Region, *Journal of Climate*, *23*(2), 419–439, 2010.

Rotunno, R., J. Klemp, and M. L. Weisman, A theory for strong, long-lived squall lines, *Journal of the Atmospheric Sciences*, *45*(3), 463–485, 1988.

Schultz, D. M., and P. N. Schumacher, The use and misuse of conditional symmetric instability, *Monthly Weather Review*, *127*(12), 2709–2732, 1999.

Schumacher, C., and R. A. Houze, Jr., Stratiform Rain in the Tropics as Seen by the TRMM Precipitation Radar*, *Journal of Climate*, *16*(11), 1739–1756, 2003.

Schumacher, C., and R. A. Houze, Jr., Stratiform precipitation production over sub-Saharan Africa and the tropical East Atlantic as observed by TRMM, *Quarterly Journal of the Royal Meteorological Society*, *132*(620), 2235–2255, 2006.

Shaw, S. B., A. A. Royem, and S. J. Riha, The Relationship between Extreme Hourly Precipitation and Surface Temperature in Different Hydroclimatic Regions of the United States, *Journal of Hydrometeorology*, *12*(2), 319–325, 2011.

Shige, S., H. Sasaki, K. Okamoto, and T. Iguchi, Validation of rainfall estimates from the TRMM precipitation radar and microwave imager using a radiative transfer model: 1. Comparison of the version-5 and -6 products, *Geophysical Research Letters*, *33*(13), L13,803, 2006.

Steiner, M., R. A. Houze, Jr., and S. E. Yuter, Climatological characterization of three-dimensional storm structure from operational radar and rain gauge data, *Journal of Applied Meteorology*, *34*(9), 1978–2007, 1995.

Tebaldi, C., K. Hayhoe, J. Arblaster, and G. Meehl, Going to the extremes, *Climatic Change*, *79*(3), 185–211, doi:10.1007/s10584-006-9051-4, 2006.

Toracinta, E. R., D. Cecil, E. Zipser, and S. Nesbitt, Radar, passive microwave, and lightning characteristics of precipitating systems in the Tropics, *Monthly Weather Review*, *130*(4), 802–824, 2002.

Trapp, R. J., N. Diffenbaugh, H. E. Brooks, M. E. Baldwin, E. D. Robinson, and J. S. Pal, Changes in severe thunderstorm environment frequency during the 21st century caused by anthropogenically enhanced global radiative forcing, *Proceedings of the National Academy of Sciences*, *104*(50), 19,719–19,723, 2007.

Trenberth, K. E., A. Dai, R. M. Rasmussen, and D. B. Parsons, The Changing Character of Precipitation, *Bulletin of the American Meteorological Society*, *84*(9), 1205–1217, 2003.

Vecchi, G., and B. Soden, Global warming and the weakening of the tropical circulation, *Journal of Climate*, *20*(17), 4316–4340, 2007.

Weisman, M. L., The role of convectively generated rear-inflow jets in the evolution of long-lived mesoconvective systems, *Journal of the Atmospheric Sciences*, *49*(19), 1826–1847, 1992.

Williams, E., et al., Contrasting convective regimes over the Amazon: Implications for cloud electrification, *J. Geophys. Res*, *107*(10.1029), 2002.

Xie, P., and P. A. Arkin, Global precipitation: a 17-year monthly analysis based on gauge observations, satellite estimates, and numerical model outputs, *Bull. Amer. Meteor. Soc.*, *78*, 2539–2558, 1997.

Zhang, C., P. Woodworth, and G. Gu, The seasonal cycle in the lower troposphere over west africa from sounding observations., *Q. J. R. Meteorol. Soc.*, *132*, 2561–2584, doi: 10.1256/qj.06.23, 2006.

Zipser, E., C. Liu, D. Cecil, S. Nesbitt, and D. Yorty, Where are the most intense thunderstorms on Earth?, *Bulletin of the American Meteorological Society*, *87*(8), 1057–1071, 2006.

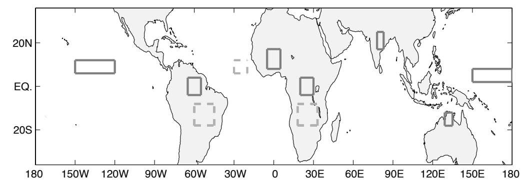

FIG. 1. Regions analyzed in this study. Dashed boxes indicate regions that were analyzed but not shown in additional figures.

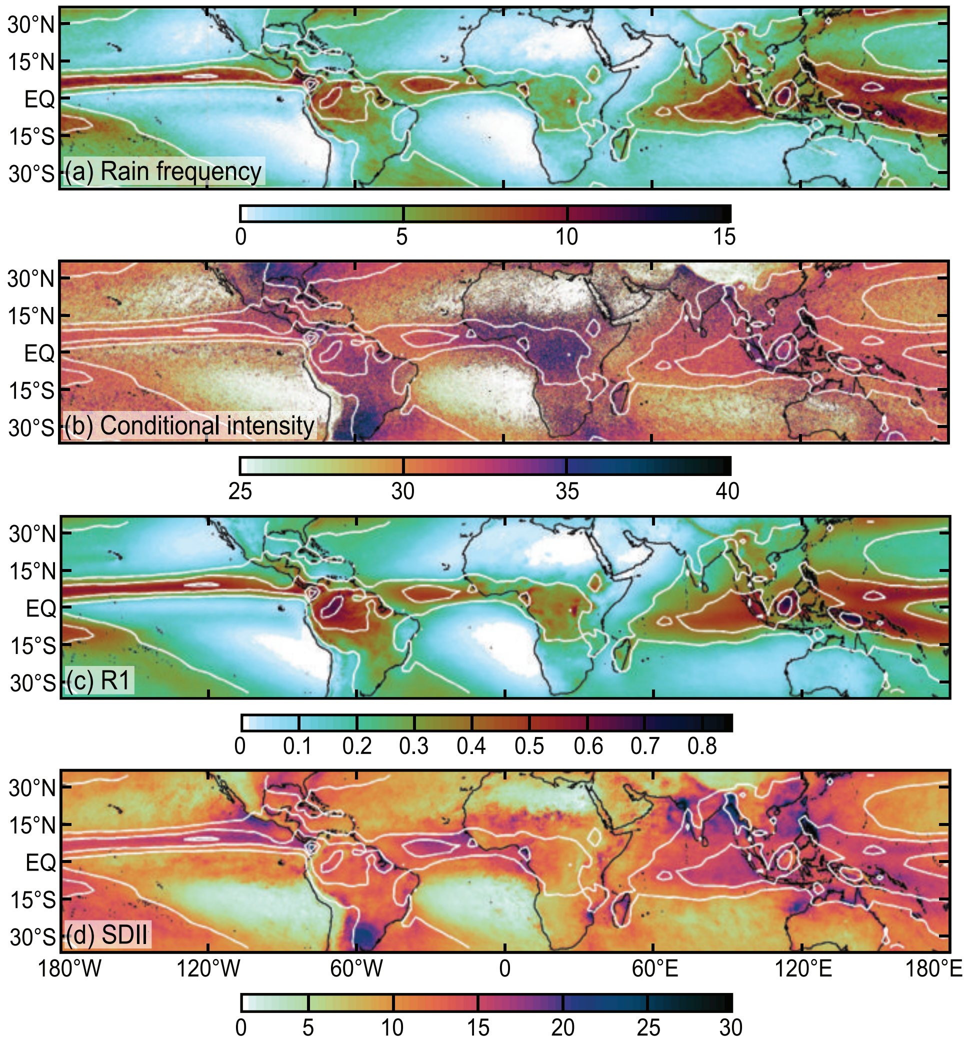

FIG. 2. The annual mean frequency and intensity maps from 1998-2007 differ when the fields are defined from instantaneous rainfall values or from diurnally aggregated rainfall values. The top panels are (a) frequency (f) and (b) intensity (i) from TRMM PR. The lower panels are (c) number of rainy days with accumulation >1 mm per day (R1) and (d) simple daily intensity index or mean rainfall accumulation on rainy days (SDII) from TRMM 3B42. Contours are annual mean rainfall rates from GPCP.

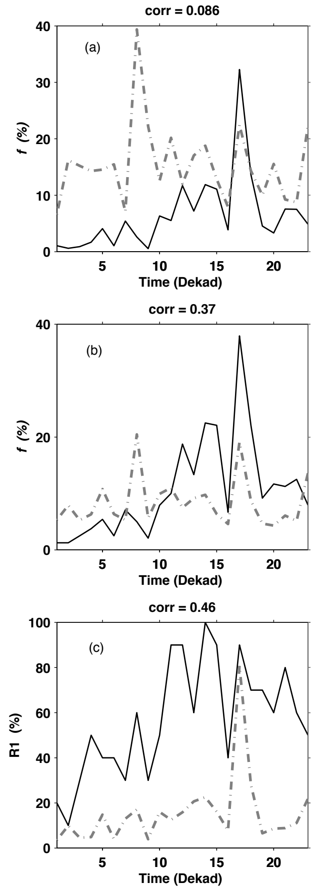

FIG. 3. Dekadal mean frequency (black, solid, in units of %) and intensity (grey, dash-dotted, in units of mm hr^{-1} in (a) and (b) and mm/day in (c)) of rainfall calculated from rain-gauge data at Darwin, Australia. (a) Minute-by-minute rainfall data (a rain event is detected for rain rates >0.4 mm hr^{-1}). (b) Hourly-mean data (a rain event is detected for rain rates>0.4 mm hr^{-1}). (c) Daily data (a rain event is detected for accumulation >1 mm/day). Dekads are counted starting from September 2010. The correlation between the frequency and intensity time series is noted in the title of each panel.

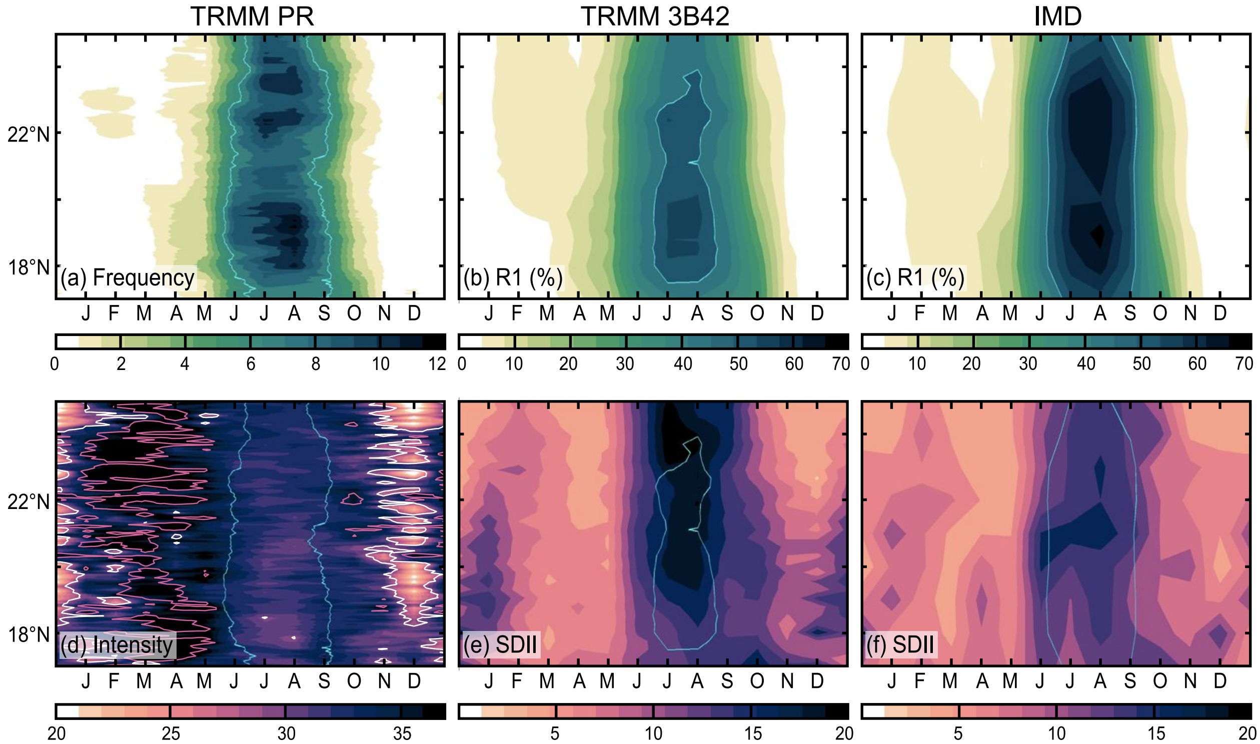

FIG. 4. Frequency (top) and intensity (bottom) of rainfall in the TRMM PR data (left), TRMM 3B42 data(center), and Indian Meteorological Department gridded station data (right), as a function of latitude and climatological month, averaged over the longitudes of central India (78^oE to 83^oE). In the left panels, frequency and intensity (f and i) calculated from snapshot values are plotted in units of % and dBZ, respectively. In the center and right panels, frequency and intensity (R1 and SDII) are plotted in units of % and mm/day, respectively. The blue contour is 7% f for instantaneous data and 50% R1 for daily data.

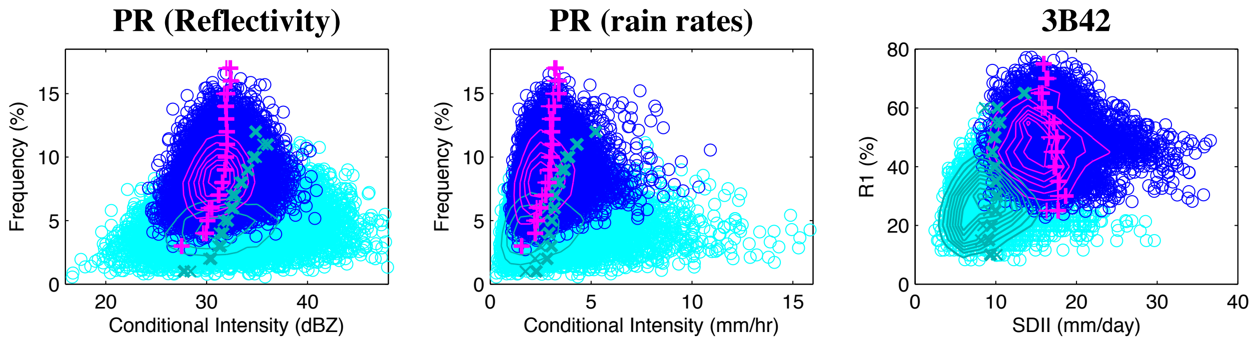

FIG. 5. Intensity/Frequency scatterplot (dots), intensity/frequency joint probability density function (contours), and mean and median intensity as a function of frequency (thick and thin symbols, respectively) for May-June (light blue) and July-August-September (dark blue and magenta) averages. The left and center panels are for TRMM PR data and consider intensity in units of reflectivity (dBZ) and rain rates (mm hr^{-1}), respectively. The right panel is for daily TRMM 3B42 data, and intensity is in units of mm/day. Data are taken from the central India box.

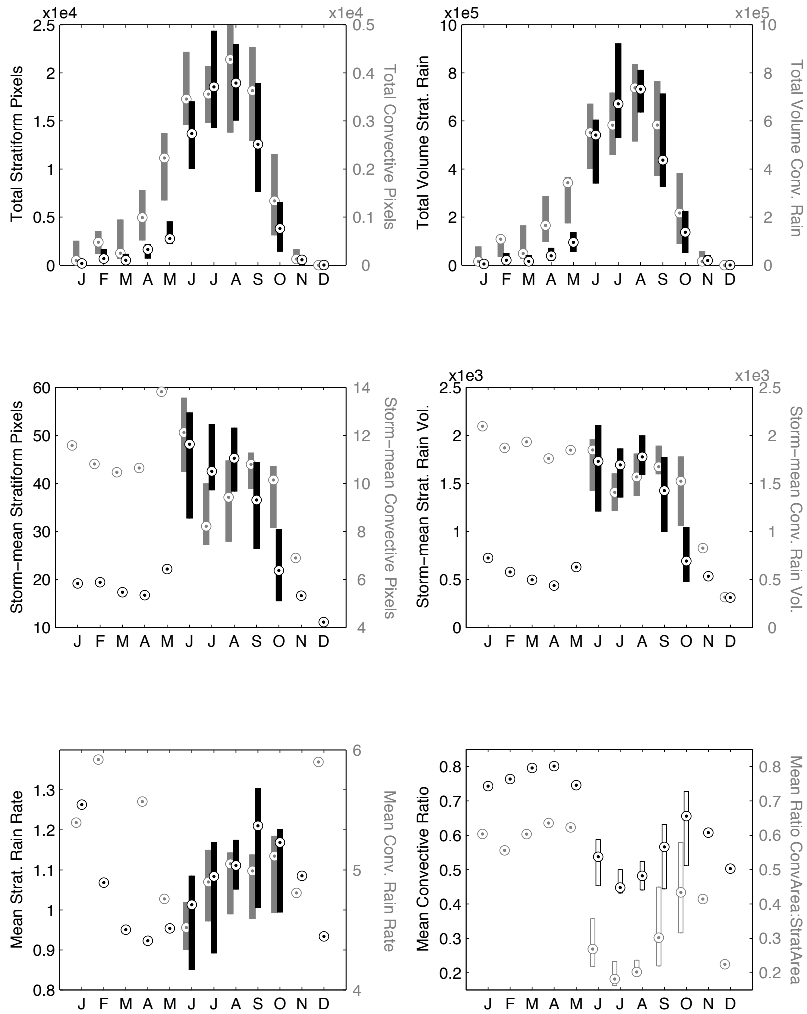

FIG. 6. Seasonal evolution of stratiform and convective rain for 1998-2007 over central India. For each variable, we plot the 25th and 75th percentile (bar) and the median values (dots) of the 10 individual monthly values. For calendar months with few rain events, only the median is plotted. Area is number of pixels. Rain is volumetric rain. Total refers to the accumulated total for the month. Storm mean is the average across the storms that happened in any given month. Mean rain per pixel is calculated as rain per storm divided by area of the storm, averaged over all the storms occurring in any given month.

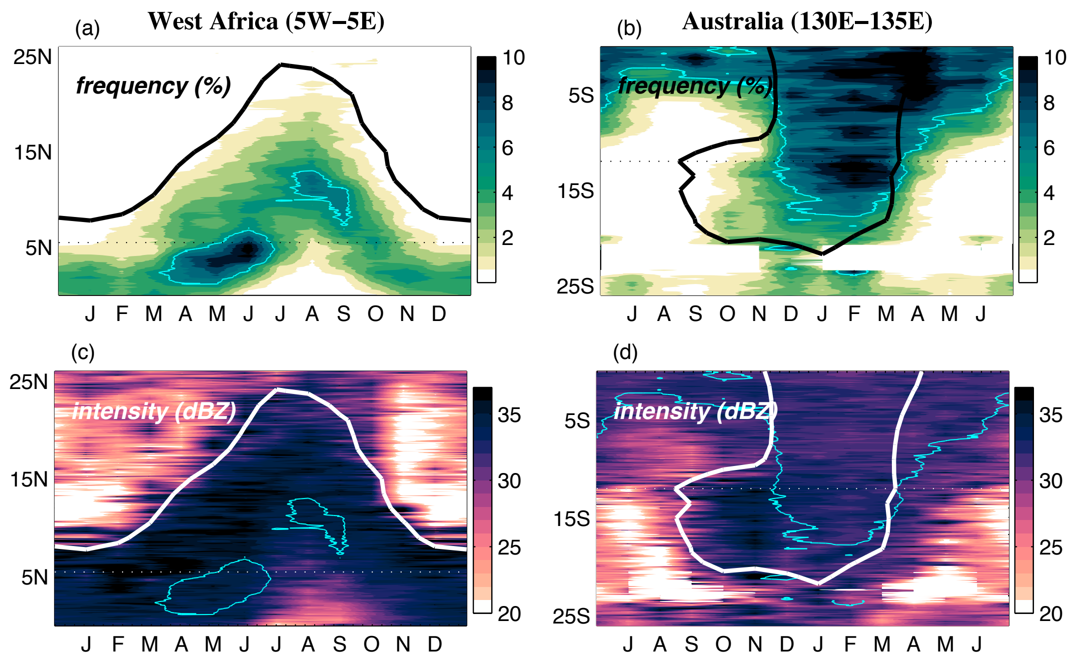

FIG. 7. As in Fig. 4-left but for (left) West Africa and (right) Australia. The thick black or white contour is the climatological surface confluence line (i.e., the line of vanishing meridional wind). Note that the calendar is shifted for Australia so that the plot is centered on the rainy season. The approximate boundary between land and ocean is denoted by the dotted lines.

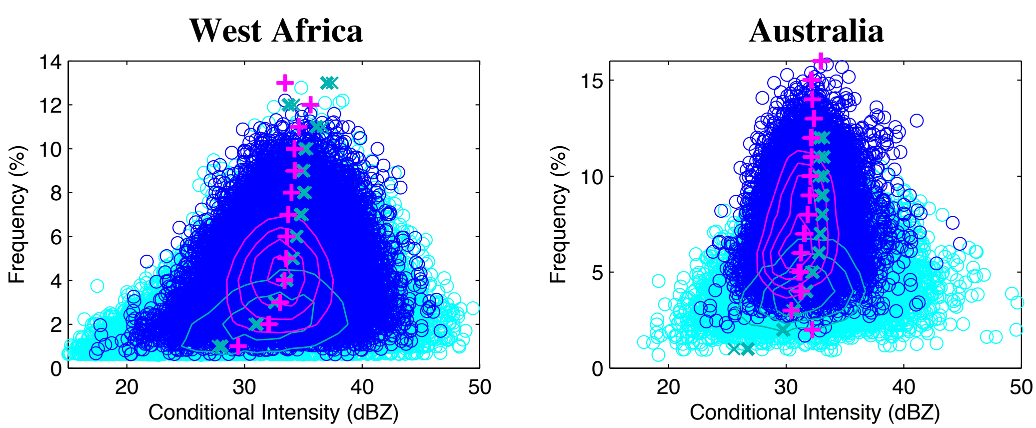

FIG. 8. As in Fig. 5-left but for (left) West Africa and (right) Australia.

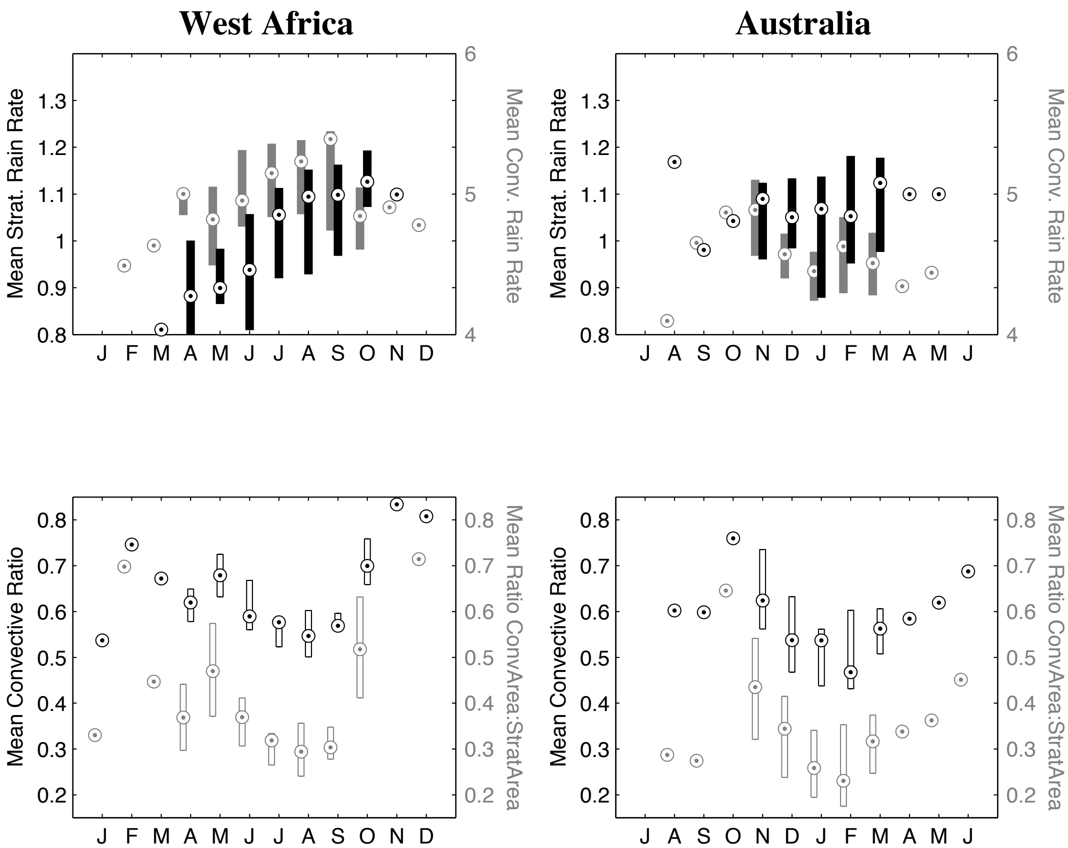

FIG. 9. As in Fig. 6-bottom but for (left) West Africa and (right) Australia. Note that the calendar is shifted for Australia so that the plot is centered on the rainy season.

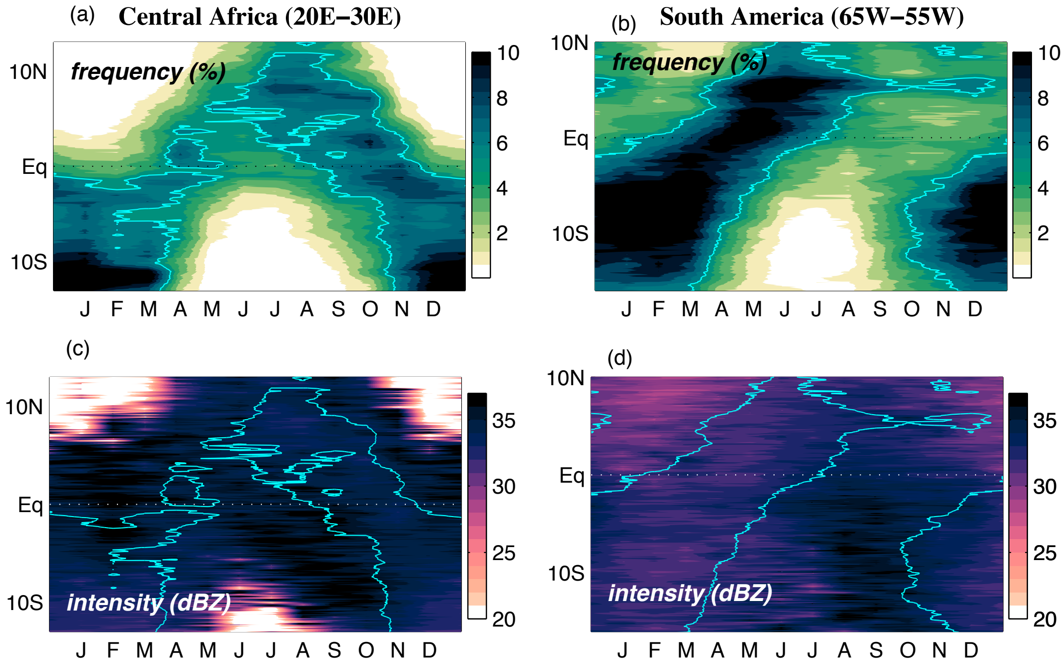

FIG. 10. As in Fig 4-left but for (left) Congo and (right) Amazon.

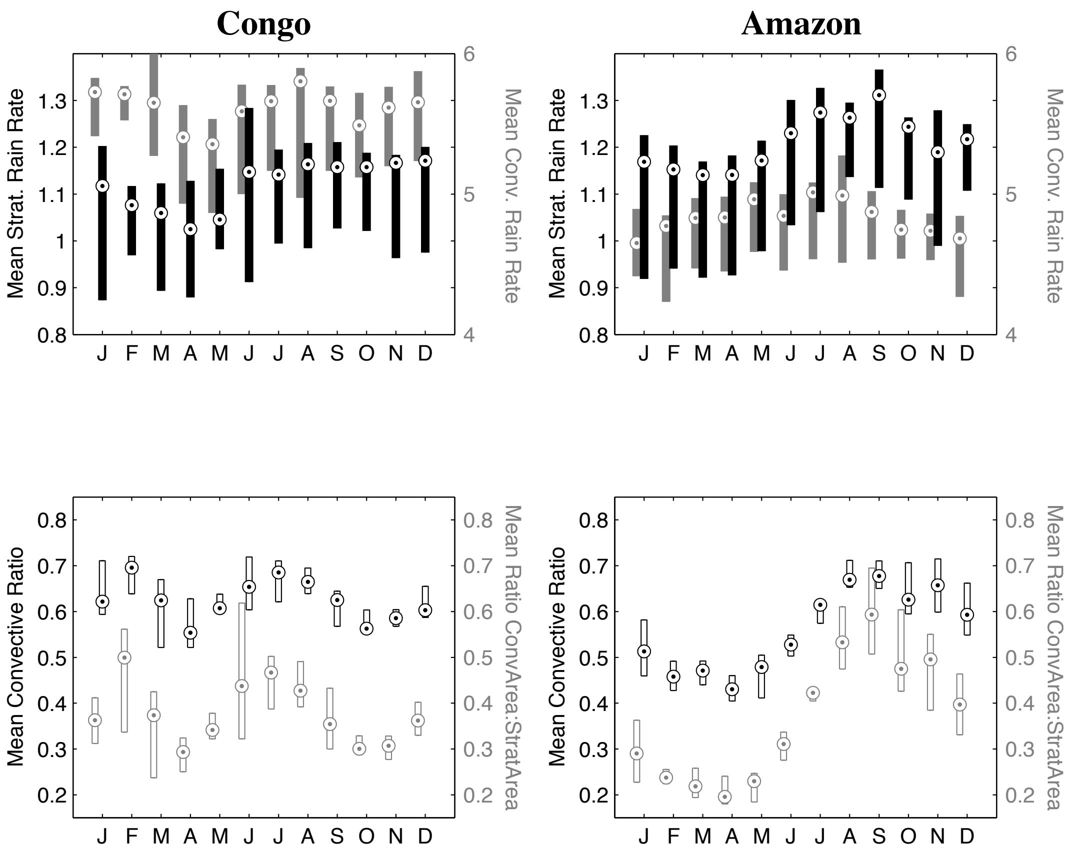

FIG. 11. As in Fig. 6-bottom but for (left) Congo and (right) Amazon.

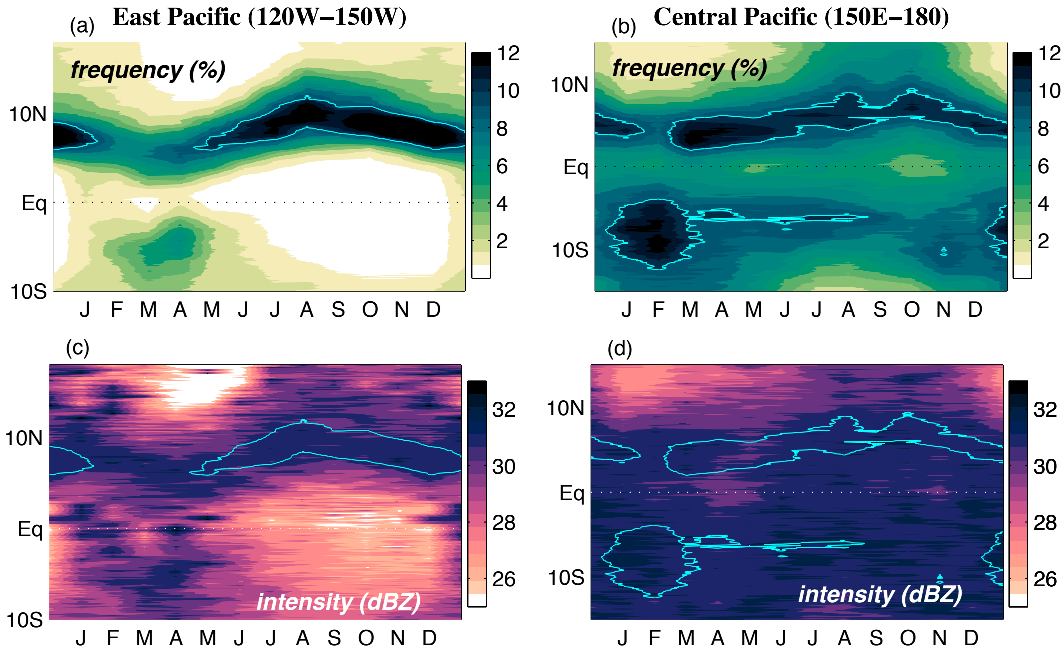

FIG. 12. As in Fig. 4-left but for (left) eastern Pacific and (right) central Pacific.

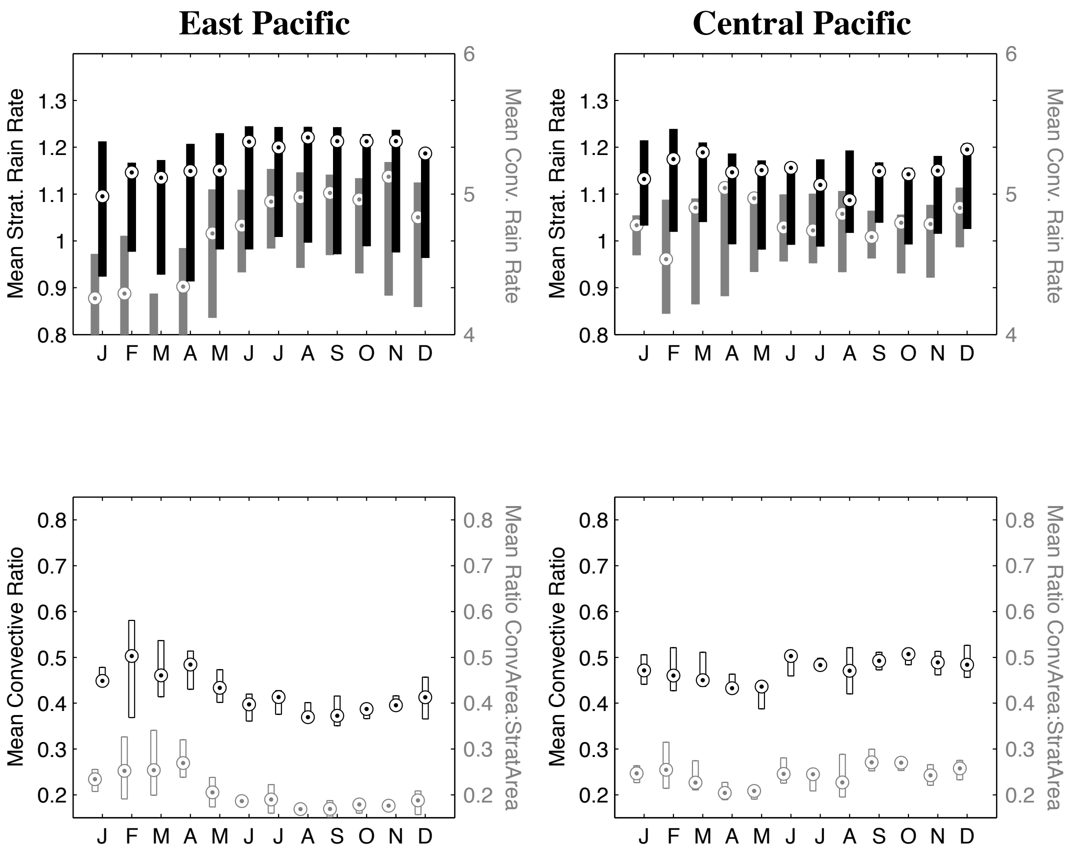

FIG. 13. As in Fig. 6-bottom but for (left) eastern Pacific and (right) central Pacific.

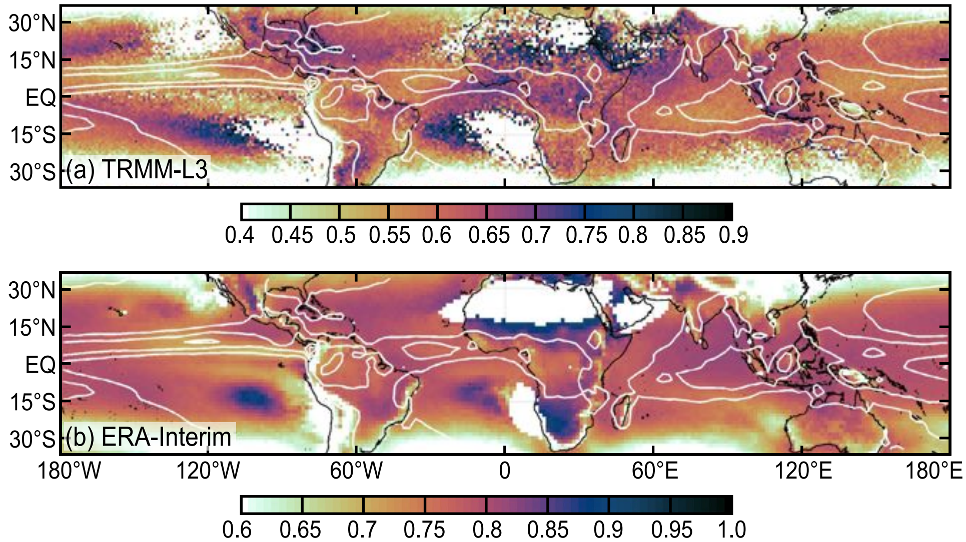

FIG. 14. Convective ratio (convective rain to total rain), calculated from (top) TRMM monthly total convective and stratiform rainfall accumulation and (bottom) ERA-Interim reanalysis daily average convective and stratiform rainfall accumulations.

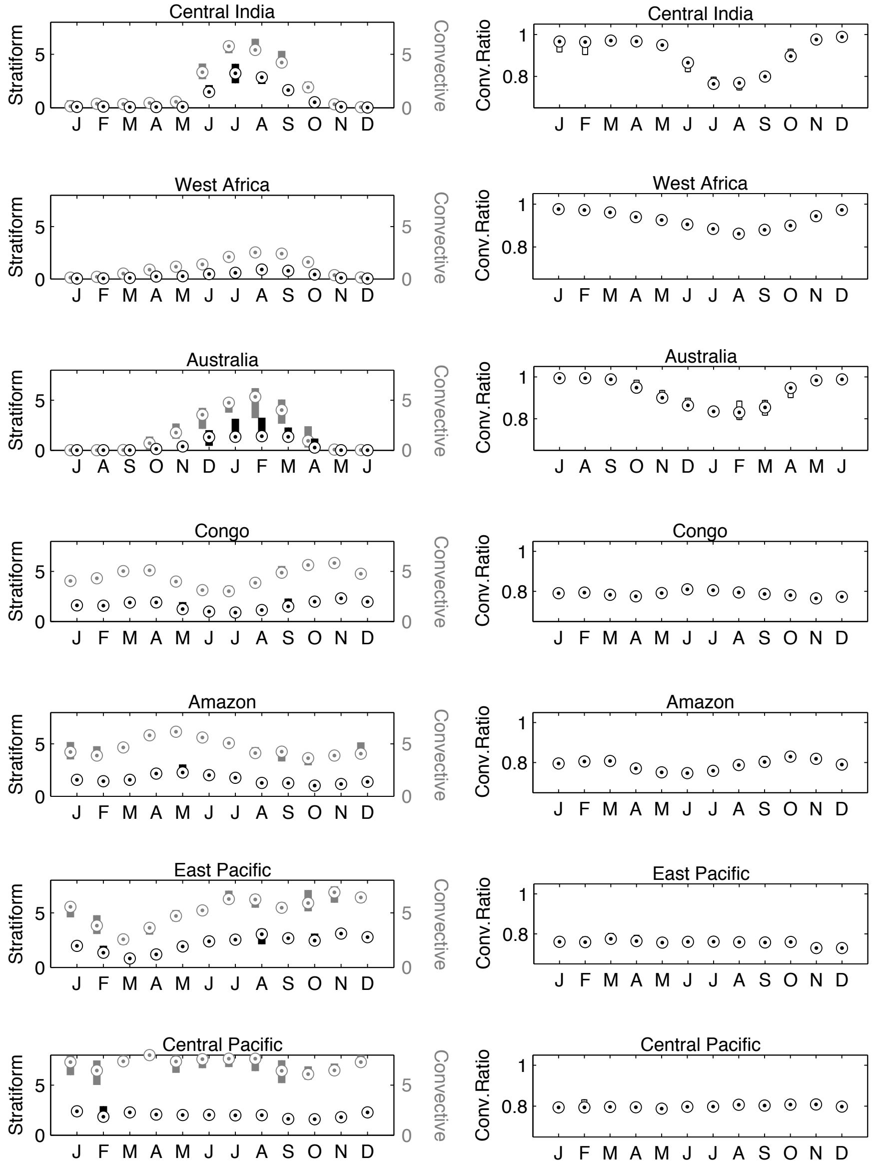

FIG. 15. Monthly (left) mean convective and stratiform rainfall and (right) convective ratio from daily values in the ERA-Interim reanalysis for different regions. See titles in each panel and Fig. 1.